MECSOL 2022 - Proceedings of the 8th International Symposium on Solid Mechanics
M.L. Bittencourt, J. Labaki, L.C.M. Vieira Jr. and E. Mesquita (Editors), Campinas SP, Brazil, October 17th to 19th, 2022

An Investigation of Hierarchical Blending Elements in G/XFEM for Linear Elasticity

Erik da R. Rodriguez[1], Oscar G. A. de Suarez[1] and Rodrigo Rossi[1]

[1] Depto. de Engenharia Mecânica, Universidade Federal do Rio Grande do Sul
Av. João Pessoa, 80, 90040-000, Rio Grande do Sul, Brazil

Abstract. This work investigates the interpolation behavior of blending elements, characterized by the non-fulfillment of partition of unity property leading to unwanted terms in the approximation and degrading the convergence rate. To deal with this issue, a hierarchical polynomial enrichment approach in blending elements is used and compared with classical XFEM, being verified by an analytical solution of a bi-material cantilever beam with a third-order displacement field, a classic engineering case, widely used in various industrial segments. The hierarchical XFEM is compared with the classical XFEM through the values of the relative error norms, convergence rate, and the local behavior of the approximate field in blending elements for two opposite material configurations with a known analytical solution. The results show that the hierarchical term enhances the approximated local field in blending elements to compensate for the unwanted terms and better approximates the local field than classical XFEM.
Keywords: XFEM, weak discontinuity, blending element, hierarchical shape functions

INTRODUCTION

The lack of accuracy and convergence rate in the finite element method (FEM) is well known when the exact solution of the partial differential equation has non-smooth behavior (Belytschko et al., 2014). According to Belytschko et al. (2009), physical problems having cracks, shear bands, inclusions, holes, shock waves, multi-phase fluids, *et cetera* need special care in FEM: mesh refinement, high-order elements, mesh conforming to the non-smooth phenomena, re-meshing for non-smooth evolution. Among several that have been used to circumvent such problems are the partition of unity-based methods — (Babuška and Melenk, 1997), (Melenk and Babuška, 1996), (Duarte and Oden, 1996), (Strouboulis et al., 2000) — that have proposed modifications in the approximation space with the aim of a more straightforward approach to non-smooth solutions, adding *a priori* knowledge of the solution or adding an extrinsic basis that aims to increase the consistency order of the approximation. These methods require specific approaches such as using appropriate numerical integration, developing an effective data structure, reducing computational cost, dealing with conditioning problems, and using special procedures for imposing boundary conditions.

Through the concept of partition of unity (PU), the generalized/extended finite element method (G/XFEM), proposed by Moës et al. (1999) and Belytschko and Black (1999), introduces the possibility of using non-polynomial terms in the approximation space to represent non-smooth phenomena such as high gradients, kinks, jumps, and singularities, not requiring the use of a mesh conforming the discontinuity interface, such as FEM. The non-smooth effects, in large part, are local phenomena, not being necessary a global enrichment of the whole approximation space, opting for enrichments in specific subdomains. In this way, G/XFEM can be considered a PU-based method with extrinsic bases added in subdomains, and due to the locality of the enrichment, the method will be referred to only as XFEM in this paper.

With the use of enrichments only in subdomains, partially enriched elements arise and do not fulfill the PU property by introducing pathological terms in the approximation space that, according to Khoei (2014), lead to poorly conditionate stiffness matrix and perturbations in the approximation fields affecting the convergence rate. Therefore, many techniques have been proposed to overcome those issues: XFEM with ridge function (Moës et al., 2003), enhanced strain XFEM and hierarchical XFEM (Chessa et al., 2003), intrinsic XFEM (Fries and Belytschko, 2006), corrected XFEM (Fries, 2008), DG-XFEM (Gracie et al., 2008), and others.

One of the two proposed techniques by Chessa et al. (2003) is the hierarchical XFEM, which utilizes different polynomials order for the standard and blending shape functions. The authors have shown that if the shape function order of the standard part is higher than the enriched part, the parasitic terms vanish. An advantage of this technique is that minor modifications in the software data structure obtain more accurate results without much more computational effort than standard XFEM.

In the present work, the blending pathological effects of the standard XFEM are compared with the blending effects of

hierarchical XFEM — HXFEM for shortness — through comparison with an analytical solution of a bi-material cantilever beam which has third-order polynomial terms in the displacement field, differing from the two classical solutions: bi-material bar with a linear solution and the inclusion bi-material problem with $1/r$ term in solution in polar coordinates. The idea is to investigate the effects of both approximation spaces, focusing on blending terms, when modeling a problem where the solution involves *a priori* higher polynomial terms in the exact solution. The comparison is made regarding the approximation spaces' numerical integration and convergence properties.

This work is organized into five sections—this introduction. Section 2 describes the main aspects of blending element error and how HXFEM circumvents it. Section 3 shows the solution of a bi-material cantilever beam with the hypothesis and conditions. Section 4 presents the numerical results and follows the conclusions in Section 5.

BLENDING ELEMENT ERROR ANALYSIS

A brief introduction to XFEM is needed to analyze the blending element error. The approximation field in XFEM can be written as

$$u(x) \approx u^h(x) = \underbrace{\sum_{i \in I} \phi_i(x)\, u_i}_{\text{approximation with intrinsic basis} \equiv \text{FEM}} + \underbrace{\sum_{j \in I^*} \Psi_j(x)\, a_j}_{\text{approximation with extrinsic basis}}, \tag{1}$$

where: $u(x)$ denotes a scalar or vectorial field; I is the set of all nodes of the mesh; I^* is the set of enriched nodes; $\phi_i(x)$ is the intrinsic basis shape function associated with the i node; u_i is the degree of freedom of the intrinsic basis; $\Psi_j(x)$ is the local enrichment function associated with the j node; a_j is the degree of freedom of the extrinsic basis.

The enrichment is constructed locally in a set $I^* \subset I$ since most of the non-smooth phenomena do not occur in the whole domain. The local characteristic of the enrichment also enhances computational efficiency. The local enrichment function has the form

$$\Psi_j(x) = \phi_j^*(x)\,\psi(x), \quad \forall j \in I^*, \tag{2}$$

where: $\psi(x)$ is the global enrichment function that includes non-smooth terms that can represent *a priori* knowledge of the solution; $\phi_j^*(x)$ must be a shape function that fulfills the PU-property

$$\sum_{j \in I^*} \phi_j^*(x) = 1, \tag{3}$$

and not necessarily needs to be the same as the chosen for the intrinsic basis, $\phi_i(x)$. The enriched elements, in which all nodes are in I^*, are obtained through the level-set method, Osher and Sethian (1988), which implicitly represents the non-smooth phenomena' geometry; in the case of bi-material problems, the non-smooth phenomena are the interface between materials. In these elements, the enrichment function reproduces exactly, $\sum_{j \in I^*} \phi_j^*(x)\,\psi(x) = \psi(x)$. However, the neighbors of enriched elements have just some nodes in I^*, and the PU-property is not satisfied, and then $\sum_{j \in I^*} \phi_j^*(x)\,\psi(x) \neq \psi(x)$. Those elements are named blending elements and introduce unwanted parasitic terms in the approximation space that can lead to poorly conditionate stiffness matrix and perturbations in the approximation fields affecting the convergence rate, (Khoei, 2014). Figure 1 shows the enriched and blending element.

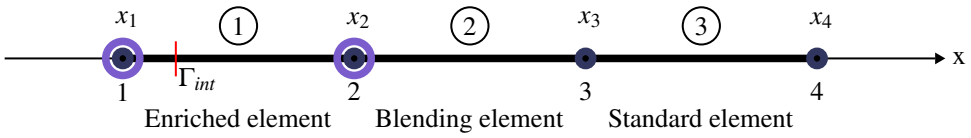

Figure 1 – Mesh of one-dimensional problem used to analyze the blending error. The enriched nodes are represented as circled dots, and the circled numbers represent the kinds of elements: 1 - Enriched element split by an interface Γ_{int}; 2 - Blending Element; 3 - Standard Element.

Following the work of Chessa et al. (2003), which analyses the influence of applying a ramp function as an enrichment function that could represent a bi-material interface in a one-dimensional problem, Tarancón et al. (2009) extends the idea to arbitrary enrichment functions. The influence in the approximation error can be obtained from an analysis of a bar discretized in three linear elements, as shown in Figure 1. Nodes 1 and 2 are enriched due to the interface Γ_{int} splitting the element. The approximation field for the blending element, circled number 2 in the Figure 1, can be written as

$$u^h(x) = u_2(1-\xi) + u_3\xi + a_2(1-\xi)\psi(x), \qquad \forall\, x \in [x_2, x_3], \tag{4}$$

where: $\xi = (x - x_2)/h$ and h is the element's size.

Chessa et al. (2003) shows that raising the polynomial order of the interpolation in the blending element improves the approximation field and, consequently, the convergence. They show this by getting *a priori* error estimate of the maximum-norm changing the enrichment function with a Taylor series expansion and, through manipulations obtaining the following inequality relation

$$\max|\Delta(x)| \leq \frac{1}{8}h^2 \max\left|\frac{d^2u}{dx^2} + \frac{2u_2}{h}\frac{d\psi}{dx}\right|, \tag{5}$$

where: $\Delta(x)$ is the approximation error that is $\Delta(x) = u(x) - u^{int}(x)$, and $u^{int}(x)$ is the approximation produced by changing the enrichment function with a Taylor series expansion which coincides with $u(x)$ at the nodes. The last term in Eq. 6, $\frac{2u_2}{h}\frac{d\psi}{dx}$ is responsible for the increase in the approximation error and does not exist in standard elements - which reproduce the same inequality as in FEM - shown in Eq. 8. Adding a quadratical hierarchical shape function to the blending element, the approximation in this element is

$$u^h(x) = u_2(1-\xi) + u_3\xi + a_2(1-\xi)\psi(x) + b_2\xi(1-\xi), \tag{6}$$

where: b_2 is the new degree of freedom associated with the quadratical hierarchical shape function. Then the inequality is

$$\max|\Delta(x)| \leq \frac{1}{8}h^2 \max\left|\frac{d^2u}{dx^2} + \frac{2a_2}{h}\frac{d\psi}{dx} + \frac{2b_2}{h^2}\right|, \tag{7}$$

and if $b_2 = -a_2 h\frac{d\psi}{dx}$, then

$$\max|\Delta(x)| \leq \frac{1}{8}h^2 \max\left|\frac{d^2u}{dx^2}\right|. \tag{8}$$

This means that increasing the polynomial order of the standard interpolation in the blending elements compensates for unwanted parasitic terms caused by partial enrichment, this could be achieved by adding hierarchical nodes. With the above results, Chessa et al. (2003) concludes that for a p-order polynomial enrichment function, if the shape function of the standard part, $\phi_i(x)$, is s-order complete and the shape function of the enriched part $\phi_j^*(x)$ is e-order complete, the spurious terms vanish when the inequality $s \geq e + p$ are fulfilled in blending elements. In two-dimensional problems, hierarchical nodes are added on the sides of the elements between enriched nodes and standard nodes, as shown in Figure 2, representing a discretized two-dimensional domain with a semi-circular interface splitting the mesh.

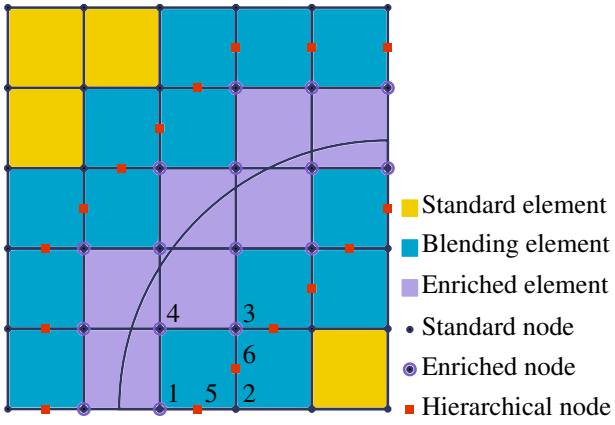

Figure 2 – A discretized two-dimensional domain with a semi-circular interface not complying with the mesh.

The approximation field, Eq. 1, can be rewritten with the additional hierarchical term being

$$u(x) \approx u^h(x) = \sum_{i\in I}\phi_i(x)\,u_i + \sum_{j\in I^*}\Psi_j(x)\,a_j + \sum_{k\in K}\hat{\phi}_k(x)\,b_k \tag{9}$$

where: K is the set of hierarchical nodes associated with the sides of the elements that connect an enriched node with a standard node.

To illustrate the addition of hierarchical shape functions, in the bottom half of Figure 2 a blending element is selected in which the nodes are numbered. In this element, there are two hierarchical nodes, and the bi-linear shapes functions in this element are

$$\phi_i(\xi,\eta) = \frac{1}{4}(1+\xi_i\xi)(1+\eta_i\eta), \qquad \text{for } i = 1,2,3,4 \tag{10}$$

and the two corresponding quadratical hierarchical shape functions are

$$\hat{\phi}_5(\xi,\eta) = \frac{1}{2}(1-\xi^2)(1-\eta) \tag{11}$$

$$\hat{\phi}_6(\xi,\eta) = \frac{1}{2}(1-\eta^2)(1+\xi) \tag{12}$$

where: ξ and η are the parent element coordinates.

ANALYTICAL SOLUTION FOR CANTILEVER BI-MATERIAL BEAM

Wang and Liu (2010) obtained an analytical solution through the Airy stress function for a bi-material beam with a graded intermediate layer that is subjected to different boundary conditions at the two ends; a specific case is a cantilever beam which will be used to evaluate the blending element behavior. The model of the cantilever bi-material beam is shown in Figure 3 with three different layers. In this section, the subscript i will be used exclusively to denote the layers, $i = 1,2,3$. The beam is subjected to a transverse force Q at the left and has a fixed end at the right. The three layers are isotropic, whose Young's moduli are E_i, and Poison's ratios are ν_i, both constants. The cross-section is rectangular with unit width and the thickness of which layer is h_i. The subsequent proceeding is detailed in Wang and Liu (2010).

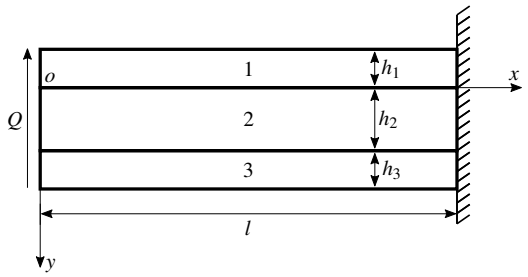

Figure 3 – Geometry, coordinates and boundary conditions of a bi-material cantilever beam.

The linear elastic problem is static with the hypothesis of plane stress without body forces; therefore, the equilibrium equations, stress-strain relations, strain-displacements relations, and the strain compatibility equation are respectively

$$\frac{\partial\sigma_{ix}}{\partial x} + \frac{\partial\sigma_{ixy}}{\partial y} = 0, \qquad \frac{\partial\sigma_{iy}}{\partial y} + \frac{\partial\sigma_{ixy}}{\partial x} = 0, \tag{13}$$

$$\varepsilon_{ix} = \frac{1}{E_i}(\sigma_{ix} - \nu_i\sigma_{iy}), \qquad \varepsilon_{iy} = \frac{1}{E_i}(\sigma_{iy} - \nu_i\sigma_{ix}), \qquad \gamma_{ixy} = \frac{2(1+\nu_i)}{E_i}\sigma_{ixy}, \tag{14}$$

$$\varepsilon_{ix} = \frac{\partial u_i}{\partial x}, \qquad \varepsilon_{iy} = \frac{\partial v_i}{\partial y}, \qquad \gamma_{ixy} = \frac{\partial u_i}{\partial y} + \frac{\partial v_i}{\partial x}, \tag{15}$$

$$\frac{\partial^2\varepsilon_{ix}}{\partial y^2} + \frac{\partial^2\varepsilon_{iy}}{\partial x^2} = \frac{\partial^2\gamma_{ixy}}{\partial x\partial y}, \tag{16}$$

where: σ_{ix}, σ_{iy}, σ_{ixy} are the stress components; ε_{ix}, ε_{iy}, γ_{ixy} are the strain components; u_i and v_i denote the displacement components.

The solution of the cantilever bi-material beam is determined through Airy stress functions ϕ_i that satisfy the equilibrium and yield a single governing equation from the compatibility statement. Then, the relation between stress and Airy stress function can be written as

$$\sigma_{ix} = \frac{\partial^2\chi_i}{\partial y^2}, \qquad \sigma_{iy} = \frac{\partial^2\chi_i}{\partial x^2}, \qquad \sigma_{ixy} = -\frac{\partial^2\chi_i}{\partial x\partial y}. \tag{17}$$

The stress function used is the polynomial

$$\chi_i = x^2 f_{i2}(y) + x f_{i1}(y) + f_{i0}(y) \tag{18}$$

where f_{i0}, f_{i1}, f_{i2} are functions to be determined.

The boundary conditions at the two ends are

$$Q = -P \quad \text{at } x = 0, \tag{19}$$

$$u_1 = 0, \qquad v_1 = 0, \qquad \frac{\partial v_1}{\partial x} = 0 \quad \text{at } (l,0). \tag{20}$$

By proceeding with the necessary replacements and manipulations with the equations shown above, the stress fields obtained from a cantilever bi-material beam with constant elastic properties are

$$\sigma_{ix} = x E_i \left(y A_{i5} + A_{i6}\right), \tag{21}$$

$$\sigma_{iy} = 0, \tag{22}$$

$$\sigma_{ixy} = -\frac{1}{2} E_i A_{i5} y^2 - E_i A_{i6} y - A_{i7}, \tag{23}$$

and the displacements

$$u_i = \frac{E_i \left(-(2+\nu_i) A_{i5} y^3 - 3\,(2+\nu_i) A_{i6} y^2 + \left(3x^2 A_{i5} - 6A_{i10}\right) y + 3A_{i6} x^2 + 6A_{i12}\right) - 12\, y A_{i7} (1+\nu_i)}{6E_i}, \tag{24}$$

$$v_i = -\frac{1}{6}\left(A_{i5} x^3 + \left(3y^2 A_{i5} \nu_i + 6y A_{i6} \nu_i - 6A_{i10}\right) x\right) + A_{i11}. \tag{25}$$

where $A_{i5} - A_{i7}$, $A_{i10} - A_{i12}$ are integral constants, that authors omitted due to the size of the equations and are shown in Wang and Liu (2010). Note that, the exact displacement solution involves third-order polynomials.

RESULTS

In order to compare the effects of blending elements in XFEM and compensated HXFEM, given by approximation Eq. 1 and Eq. 9, respectively, the bi-material cantilever beam problem was solved, for both, with: shifted absolute enrichment function $\psi_j(x) = \gamma(x) - \gamma(x_j)$, $\forall j \in I^*$, constructed with signed distance function $\gamma(x)$; and bilinear Lagrangian shape functions in standard and enriched parts, becoming $\phi(x) = \phi^*(x)$. For the compensation interpolation term from HXFEM, the hierarchical quadratic Lagrangian shape functions are used in the blending parts, $\hat{\phi}(x)$.

The numerical integration was performed in two ways: using the Gauss-Legendre quadrature with 36 points and sub-cells integrations conforming to the bi-material interfaces resulting in 24 points.

The geometry sizes and elastic properties of layers 1 and 3 are the same; the length of the cantilever is $l = 5$, the height is unitary, with the layer's height being $h_1 = h_3 = 0.25$, and $h_2 = 0.5$.

The Cartesian meshes are discretized and linearly refined with the sizes $n_x^{el} \times n_y^{el}$, where $n_x^{el} = [30, 50, 70, 90, 110]$ and $n_y^{el} = [6, 10, 14, 18, 22]$ are the numbers of elements per direction. The interfaces are localized, splitting the middle of the elements.

Two cases with different materials properties combinations are analyzed:

- Case 1: Which can represent a coating structure with two soft outer films with $E_1 = E_3 = 100$, $\nu_1 = \nu_3 = 0.25$, and the hard core with $E_2 = 500$ and $\nu_2 = 0.3$;
- Case 2: Which can represent a sandwich beam with two rigid external skins with $E_1 = E_3 = 500$, $\nu_1 = \nu_3 = 0.3$, and the soft core $E_2 = 100$ and $\nu_2 = 0.25$;

For the sake of shortness, abbreviations are defined that combine the approximation fields and the integrations used, according to Table 1.

Some error measures are defined to verify the solutions. The energy norms can be defined as $\|u^h\|_{E(\Omega)} = a(u^h, u^h)_\Omega^{1/2}$ and the L^2-displacement norm as $\|u^h\|_{L^2(\Omega)} = (u^h, u^h)_\Omega^{1/2}$. The relative error concerning the energy norm $e_{E(\Omega)}$ and L_2-displacement norm $e_{L^2(\Omega)}$ are respectively defined as

$$e_{E(\Omega)} = \frac{\|u - u^h\|_{E(\Omega)}}{\|u\|_{E(\Omega)}}, \qquad e_{L_2(\Omega)} = \frac{\|u - u^h\|_{L_2(\Omega)}}{\|u\|_{L_2(\Omega)}}. \tag{26}$$

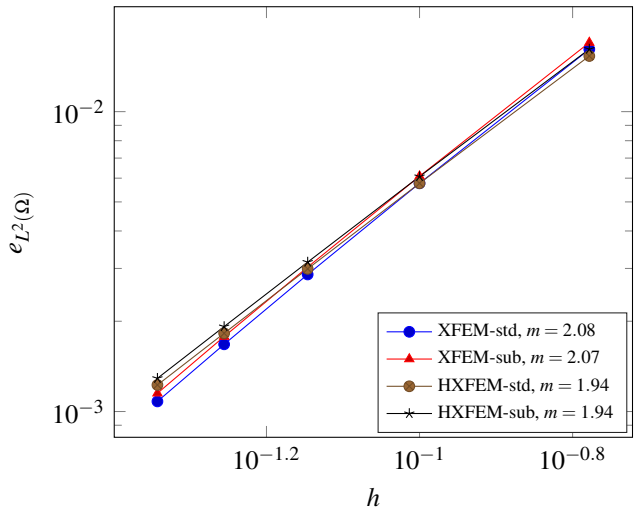

(a) Case 1: Relative L^2-displacement norm.

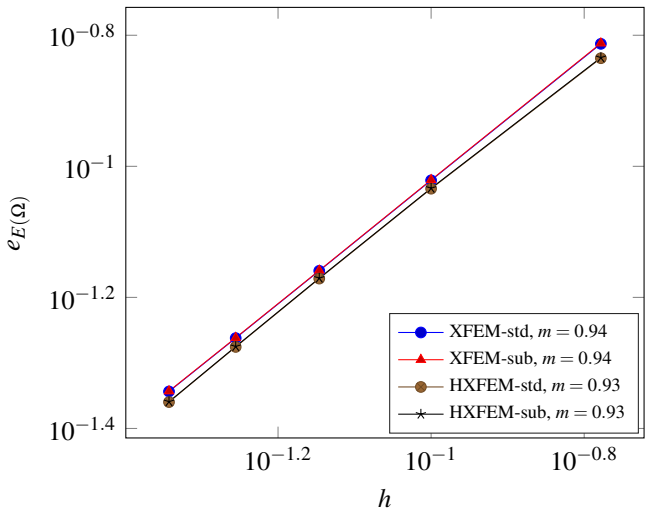

(b) Case 1: Relative energy norm.

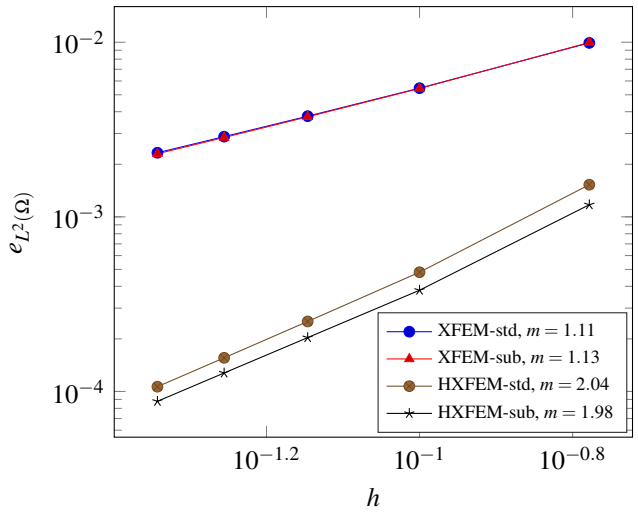

(c) Case 2: Relative L^2-displacement norm.

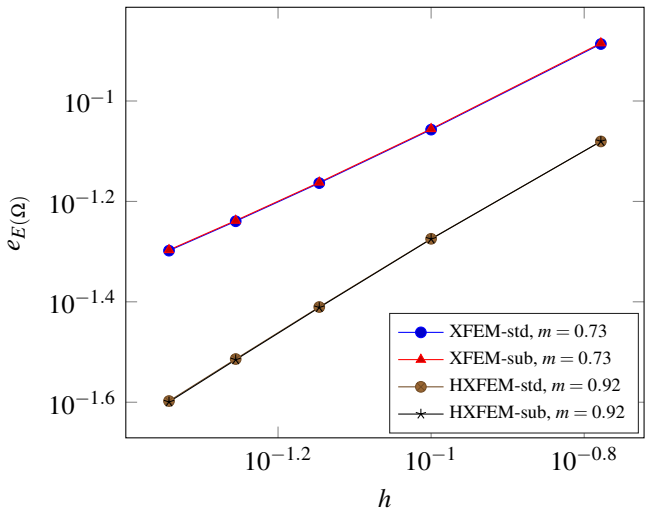

(d) Case 2: Relative energy norm.

Figure 4 – Relative norms behavior for Case 1 and 2.

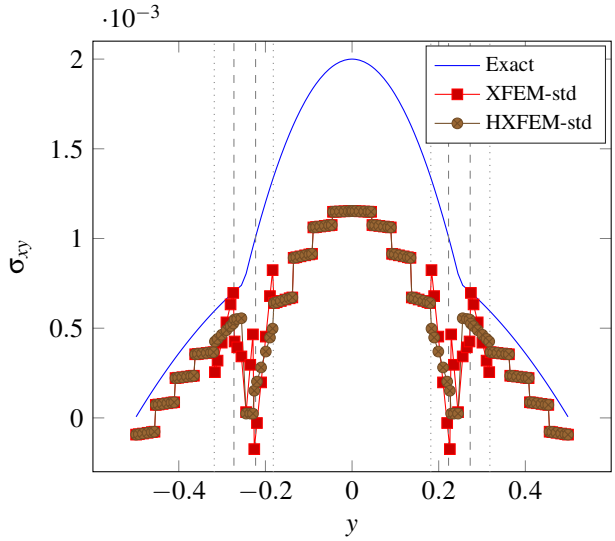

(a) Case 1: Stress field σ_{xy}.

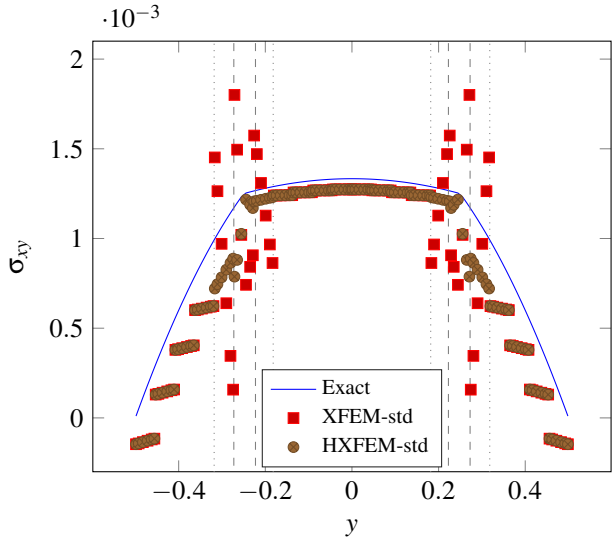

(b) Case 2: Stress field σ_{xy}.

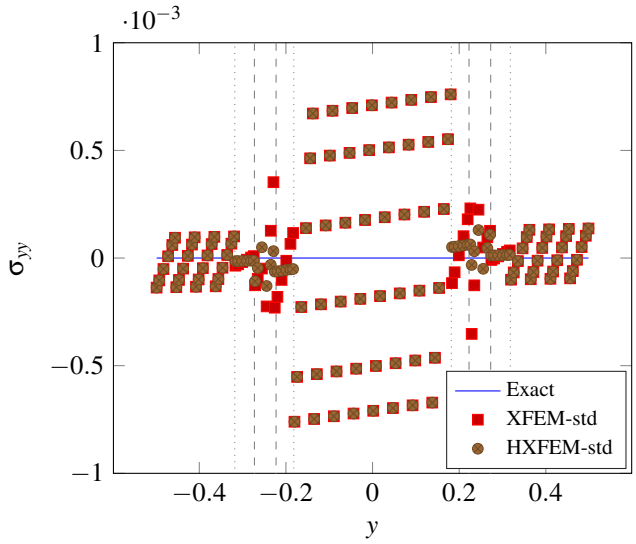

(c) Case 1: Stress field σ_{yy}.

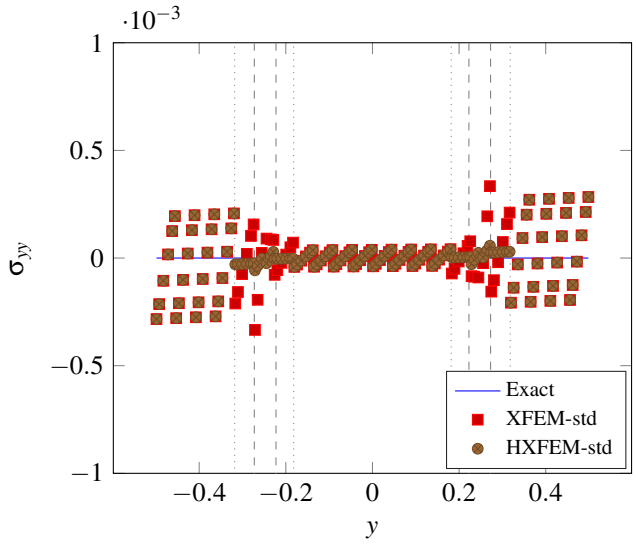

(d) Case 2: Stress field σ_{yy}.

Figure 5 – Stress fields σ_{xy} and σ_{yy} obtained from a slice nearly to $x = l/2$ in a mesh of size $n_x^{el} \times n_y^{el} = 110 \times 22$ for Case 1 and 2. The dashed vertical lines represent the edges of the enriched elements, and the dotted vertical lines and the adjacent dashed lines form the edges of the blending elements.

Table 1 – Abbreviations that combine the approximation fields and integration types.

Abbreviation	Approximation Field	Integration
XFEM-std	Eq. 1	standard as in FEM
XFEM-sub	Eq. 1	sub-cells
HXFEM-std	Eq. 9	standard as in FEM
HXFEM-sub	Eq. 9	sub-cells

To begin the investigation of the results, a mesh with size $n_x^{el} \times n_y^{el} = 50 \times 10$ was selected to analyze the approximated stress fields for Case 1 qualitatively. The result obtained for the stress field σ_{xx} is shown in Fig. 6, which presents stress concentrations in the hard core, layer 2, nearly the fixed end with the maximum absolute value of $\sigma_{xx} = 0.043988$; this behavior is expected because layers 1 and 3 are soft than layer 2. Furthermore, Figure 7 shows the stress field σ_{yy}, which presents non-null fields differing from the analytical solution, given by Eq. 22, with zero value. The maximum absolute value for this field is $\sigma_{yy} = 0.0016277$, being one order of magnitude less than σ_{xx}. Moreover, Figure 8 shows the stress field σ_{xy}, which exhibits apparent parabolic behavior concerning the y-axis in the domain, varying only close to the prescribed boundaries differing from the analytical solution, Eq. 23, which does not vary with x. These variations can be justified through Saint Venant's principle in which the stress fields near the ends are influenced by the exact local traction distribution and should decay with distance from then. The analytical solution provided here does not consider these effects, which could allow a better representation of the field in this region.

Solving the cases for all defined meshes, the convergence plots for the relative norms, as the h of the elements decreases, were obtained and are shown in Fig. 4. Furthermore, an analysis of the evolution of approximated stress fields σ_{xy} and σ_{yy} are done in y-direction taken from the integration points from a slice nearly to $x = l/2$ in a mesh of size $n_x^{el} \times n_y^{el} = 110 \times 22$; these results are shown in Figure 5.

Overall, for both cases, the relative L^2-displacement norm did not present any behavior pattern besides the linear convergence rate in the logarithmic scale. In contrast, improvements were observed in the values in the relative energy norm, and there was no considerable difference in the type of integration for this norm.

In Case 1, the relative L^2-displacement norm, shown in Fig. 4a, did not present a conclusive pattern about which is significantly better, only that the convergence rates did not vary substantially with the kind of integrations. Thus, for XFEM, the rate was around $m = 2.08$, and for HXFEM of $m = 1.94$, a relative worsening of 7%.

The HXFEM values of the relative energy norm, shown in Fig. 4b, were slightly better, and there is no significant difference between the convergence rates, which were at $m = 0.94$ and $m = 0.93$, for XFEM and HXFEM, respectively.

For XFEM-std and HXFEM-std, it can be seen in Fig. 5a that the stress field σ_{xy} does not reproduce the steep behavior of the core as in the exact solution, appearing to be translated to low values than the exact solution. This could be improved with the p-refinement or by h-refinement, since the problem has convergent characteristics.

In Case 2, HXFEM performed better regarding values and convergence rate in both norms, with subcell integration showing better values than the standard in the relative displacement norm L^2. In terms of convergence rate, there are no notable differences in the type of integrations used, so the values shown below are the average convergence rate between both integrations, with the exact values shown in the legends of Fig. 4c and Fig. 4d. The relative L^2-displacement norm showed a convergence rate for XFEM around $m = 1.12$ and HXFEM around $m = 2.01$, equivalent to a relative improvement of approximately 44%. Furthermore, the energy norm had a relative improvement of 20.6%, between XFEM and HXFEM, with the convergence rates of $m = 0.73$ and $m = 0.92$, respectively.

Figure 5b shows the σ_{xy} for this case, differing from Case 1, the approximation field is better reproduced given the plateau behavior of the core, which facilitates the approximation. In the same way, as in Case 1, the HXFEM-std does not show oscillation in blending elements like the XFEM-std.

The approximated stress field σ_{yy}, shown in Fig. 5c and Fig. 5d, presents some oscillatory behavior with smaller amplitude in blending elements, which could be justified in both cases by the approximation space orders in contrast with the polynomial order of the exact fields.

Given all the results, it can be seen that the similarity between the relative norms for both approximation fields in Case 1 can be justified probably by the lack of reproducibility of the exact stress field σ_{xy}, controlling the error more than the blending effects, needing further h-refinement to interpolate the fields better. In Case 2, due to the stress field σ_{xy} being better behaved, the blending element starts to command the convergence rate, and the resulting spurious terms in XFEM are evident. Another interesting result in HXFEM is the better interpolation of the fields in blending elements than the standard, which is justified by adding the hierarchical quadratic term and compensating for the spurious terms, and better interpolating the stress fields. Note that the approximation space is constructed with bilinear Lagrangian shape

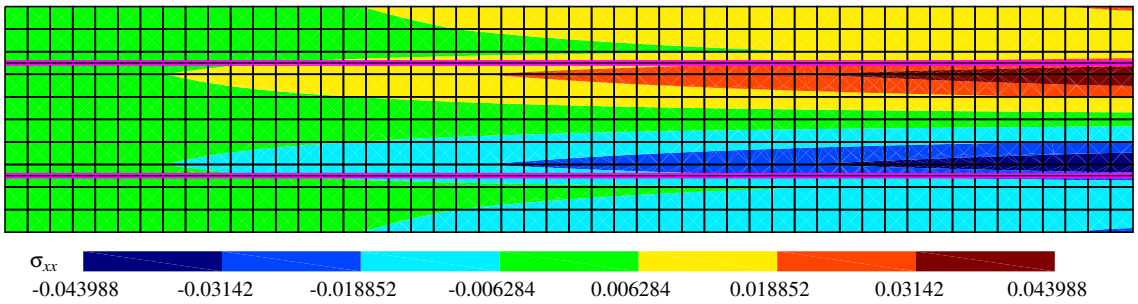

Figure 6 – Stress field σ_{xx} for a mesh size 10x50 in case of HXFEM-std.

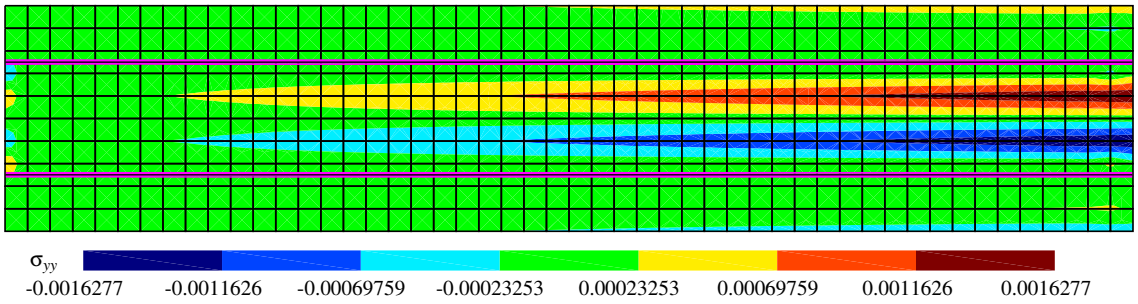

Figure 7 – Stress field σ_{yy} for a mesh size 10x50 in case of HXFEM-std.

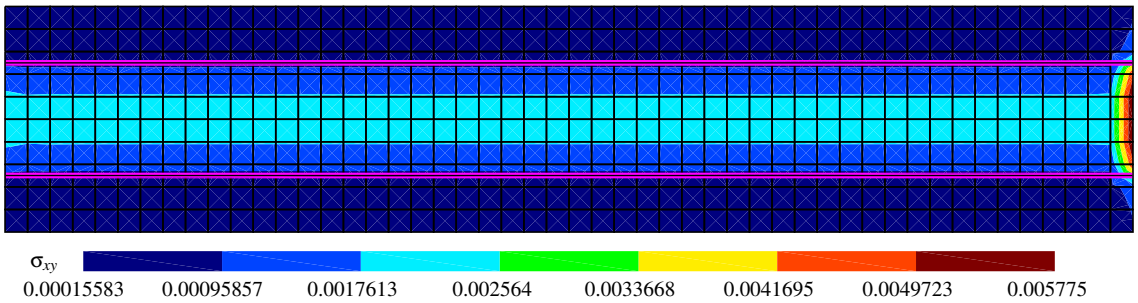

Figure 8 – Stress field σ_{xy} for a mesh size 10x50 in case of HXFEM-std.

functions and quadratic local enrichment functions on the enriched elements, given by Eq. 2, which does not guarantee the continuity between elements in the stress fields.

Thus, to even better approximate the bi-material cantilever beam, a possibility is to use the idea of the hierarchical element to raise the order of the approximation, respecting inequality between the polynomial orders of the intrinsic and extrinsic bases not adding unwanted terms.

CONCLUSION

This work investigated the interpolation behavior of blending elements in a bi-material cantilever beam with a third-order displacement field for the hierarchical XFEM. Compared with the standard XFEM, the hierarchical XFEM results show a better interpolation of the fields in the blending elements than other elements; this is justified by the addition of the hierarchical quadratic term, compensating for the spurious terms, and better interpolating the stress fields, leading in some cases better values and/or convergence rates in the relative norms of L^2-displacement and energy. However, to even better approximate high-order problems, the idea of the hierarchical element can be used to raise the order of the approximation without much effort, which may be a topic for future studies.

ACKNOWLEDGMENTS

The support of the UFRGS, CAPES, and FAPERGS for financial research support. Grant numbers: CNPq 309430/2021-6, FAPERGS: 19/2551-0001954-8-1.

REFERENCES

I. Babuška and J. M. Melenk. The Partition of Unity Method. *International Journal for Numerical Methods in Engineering*, 40(4):727–758, 1997. ISSN 1097-0207. doi: 10.1002/(SICI)1097-0207(19970228)40:4<727::AID-NME86>3.0.CO;2-N.

T. Belytschko and T. Black. Elastic crack growth in finite elements with minimal remeshing. *International Journal for Numerical Methods in Engineering*, 45(5):601–620, 1999. ISSN 1097-0207. doi: 10.1002/(SICI)1097-0207(19990620)45:5<601::AID-NME598>3.0.CO;2-S.

Ted Belytschko, Robert Gracie, and Giulio Ventura. A review of extended/generalized finite element methods for material modeling. *Modelling and Simulation in Materials Science and Engineering*, 17(4):043001, Jun 2009. ISSN 0965-0393, 1361-651X. doi: 10.1088/0965-0393/17/4/043001.

Ted Belytschko, W. K. Liu, B. Moran, and Khalil I. Elkhodary. *Nonlinear finite elements for continua and structures*. Wiley, Chichester, West Sussex, United Kingdon, second edition, 2014. ISBN 9781118632703.

Jack Chessa, Hongwu Wang, and Ted Belytschko. On the construction of blending elements for local partition of unity enriched finite elements. *International Journal for Numerical Methods in Engineering*, 57(7):1015–1038, Jun 2003. ISSN 0029-5981, 1097-0207.

C. Armando Duarte and J. Tinsley Oden. An h-p adaptive method using clouds. *Computer Methods in Applied Mechanics and Engineering*, 139(1):237–262, December 1996. ISSN 0045-7825. doi: 10.1016/S0045-7825(96)01085-7.

Thomas-Peter Fries and Ted Belytschko. The intrinsic xfem: a method for arbitrary discontinuities without additional unknowns. *International Journal for Numerical Methods in Engineering*, 68(13):1358–1385, Dec 2006. ISSN 00295981, 10970207. doi: 10.1002/nme.1761.

Thomas-Peter Fries. A corrected xfem approximation without problems in blending elements. *International Journal for Numerical Methods in Engineering*, 75(5):503–532, Jul 2008. ISSN 00295981, 10970207. doi: 10.1002/nme.2259.

Robert Gracie, Hongwu Wang, and Ted Belytschko. Blending in the extended finite element method by discontinuous galerkin and assumed strain methods. *International Journal for Numerical Methods in Engineering*, 74(11): 1645–1669, Jun 2008. ISSN 00295981, 10970207. doi: 10.1002/nme.2217.

Amir R. Khoei. *Extended Finite Element Method: Theory and Applications*. Wiley, first edition, 2014.

J. M. Melenk and I. Babuška. The partition of unity finite element method: Basic theory and applications. *Computer Methods in Applied Mechanics and Engineering*, 139(1):289–314, December 1996. ISSN 0045-7825. doi: 10.1016/S0045-7825(96)01087-0.

Nicolas Moës, John Dolbow, and Ted Belytschko. A finite element method for crack growth without remeshing. *International Journal for Numerical Methods in Engineering*, 46(1):131–150, 1999. ISSN 1097-0207. doi: 10.1002/(SICI)1097-0207(19990910)46:1<131::AID-NME726>3.0.CO;2-J.

N. Moës, M. Cloirec, P. Cartraud, and J.F. Remacle. A computational approach to handle complex microstructure geome-

tries. *Computer Methods in Applied Mechanics and Engineering*, 192(28–30):3163–3177, Jul 2003. ISSN 00457825. doi: 10.1016/S0045-7825(03)00346-3.

Stanley Osher and James A Sethian. Fronts propagating with curvature-dependent speed: Algorithms based on Hamilton-Jacobi formulations. *Journal of Computational Physics*, 79(1):12–49, November 1988. ISSN 0021-9991. doi: 10.1016/0021-9991(88)90002-2.

T. Strouboulis, I. Babuška, and K. Copps. The design and analysis of the Generalized Finite Element Method. *Computer Methods in Applied Mechanics and Engineering*, 181(1):43–69, January 2000. ISSN 0045-7825. doi: 10.1016/S0045-7825(99)00072-9.

J. E. Tarancón, A. Vercher, E. Giner, and F. J. Fuenmayor. Enhanced blending elements for xfem applied to linear elastic fracture mechanics. *International Journal for Numerical Methods in Engineering*, 77(1):126–148, Jan 2009. ISSN 00295981, 10970207. doi: 10.1002/nme.2402.

Meiqin Wang and Yihua Liu. Analytical solution for bi-material beam with graded intermediate layer. *Composite Structures*, 92(10):2358–2368, Sep 2010. ISSN 02638223. doi: 10.1016/j.compstruct.2010.03.013.

RESPONSIBILITY NOTICE

The authors hereby confirm that they are the sole liable persons responsible for the authorship of this work, and that all material that has been herein included as part of the present paper is either the property (and authorship) of the authors, or has the permission of the owners to be included here.